Photonic Millimeter-Wave Bridge for Multi-Gbps Passive Optical Networks

Ivan Aldaya[1], Carolina Del-Valle-Soto[2], Gabriel Campuzano[3], Elias Giacoumidis[4], Rafael González[3], Gerardo Castañón[3]

Abstract

Survivability is a critical requirement of optical communication networks that is typically addressed implementing path diversity. However, due to the elevated cost of fiber installation, this approach may prove prohibitively expensive in optical access networks. In this paper, a novel cost-efficient photonic millimeter (mm) - wave bridge is proposed, which converts passive optical network (PON) signals to radiofrequency signals at mm-wave bands. The performance of the mm-wave photonic bridge is numerically tested, revealing its feasibility to transmit a 2.5-Gbps PON with –55.6 dB wireless link gain (WLG) using the 81-86 GHz band and 10-Gbps PON with –35 dB at the 102-109.5 GHz band. The effect of fiber is also analyzed, showing that fiber cuts closer to the optical network unit degrades more the system performance.

Keywords: Passive Optical Networks, mm-Wave Links, Network Survivability

1. Introduction

Optical fiber has emerged as the only transmission technology capable of meeting the increasing capacity requirement not only in long-haul links, but also in metropolitan and access networks [1]. In this context, passive optical

*Corresponding author
Email address: ivan.aldaya@sjbv.unesp.br (Ivan Aldaya)
[1]Sao Paulo State University, Campus Sao Joao da Boa Vista, SP.
[2]Universidad Panamericana. Facultad de Ingeniería. Prolongación Calzada Circunvalación Poniente 49, Zapopan, Jalisco, 45010, Mexico.
[3]Engineering School, Tecnologico de Monterrey, Mexico.
[4]Dublin City University, Dublin, Ireland.

networks (PONs), where the signal is transmitted through an optical distribution network without amplification, have emerged as a cost-efficient technology and are being deployed all around the world to offer higher transmission rates to the end user [2]. PON standards have evolved to adapt to user demands [3], from the obsolete 155-Mbps broadband PON standard to Gigabit PON (G-PON) [4] and state-of-the-art XG-PON [5] operating at 2.5 and 10 Gbps, respectively. Furthermore, PON became a key enabling technology supporting backhaul in already deployed 3G cellular systems and future 4G and 5G systems [6]. However, deployment of PON networks is sometimes complicated due to urban architecture or geographical constraints, specially in vast countries such as Australia or Mexico. In addition, PON networks are very sensitive to seismic and other natural catastrophes as shown by the devastating earthquake in Japan in 2011 [7, 8]. Given the dependency of most services on internet connection, this earthquake revealed a critical Achille's heel in existing optical networks, including those supporting the emergency management.

Survivability is a key feature of any network design, but in the particular case of optical networks, is even more important due to the great amount of transmitted data and the difficult fiber repair process. In long-haul optical links, vulnerability to accidental fiber cuts is addressed through self-healing topologies, such as ring-based schemes or spatial diversity [9]. But these approaches may result prohibitively expensive in optical access networks where the cost associated to fiber installation represents the mayor part of the implementation expenses [10, 11]. An attractive alternative consists on using a wireless bridge, that is, a point-to-point wireless connection, communicating two fiber spans [7, 8, 12, 13]. Because of the high bitrate of the transmitted signal, this wireless bridge can only operate at millimeter-wave (mm-wave) frequencies, where huge unlicensed bands are still underutilized [14]. In [12], electrical means are used to generate a signal at 220 GHz suitable for radiation, whereas in [7] and in [13], the signal is generated in a centralized fashion using a typical radio over fiber (RoF) approach [15]. The former offers the possibility to change the properties of the signal, optimizing and adapting the modulation format to the

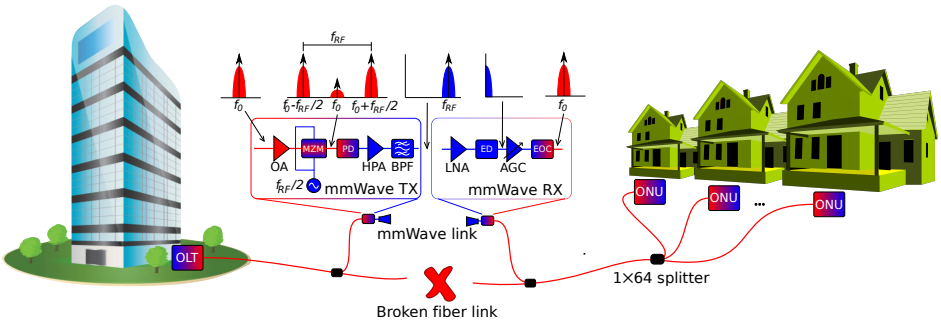

Figure 1: PON network employing the proposed photonic mm-wave bridge. OLT: optical line terminal, ONU: optical network unit, OA: optical amplifier, MZM: Mach-Zehnder modulator, PD: photodetector, BPF: bandpass filter, LNA: low-noise amplifier, FDC: frequency downconverter, AGC: automatic gain control, EOC: electrooptical converter.

wireless channel, but it requires high-frequency components and electronics with broad-bandwidth signal processing capabilities, increasing not only the cost but also the power consumption. In addition, the electrical demodulation, modulation, and up-conversion processes induce a time latency that may degrade the transmission performance. On the other hand, the RoF approach requires lower bandwidth electronics and causes minimal latency, but it lacks control on the modulation format of the radiated signal and, since there is not signal regeneration, the effects of the impairments both in the fiber and wireless channels are accumulated. In addition, in the schemes presented in [7] and in [8], as in many RoF schemes, the high-frequency RF signal is generated by photo-detecting an optical signal that has a bandwidth much broader than that of a typical PON signal. Since this signal is generated in the ONT, it must traverse all the optical network up to the fiber cut, which may result in bandwidth incompatibility. Even more, since the RoF signal has to travel from the ONT to the fiber cut, it is affected by the fiber chromatic dispersion.

In this paper we present a novel photonic mm-wave bridge based on RF frequency doubling, which is shown in Fig. 1. The incoming optical signal is amplified and remodulated using a Mach-Zehnder modulator (MZM) before being detected by a broad-bandwidth photodetector (PD). Afterwards, the photo-

generated signal is amplified using a high-power amplifier (HPA) and radiated. In the wireless receiver, the mm-wave signal is downconverted to baseband and converted back to the optical domain. In comparison to [12], the number of high-frequency devices is significantly lower and the required frequency of the oscillator is reduced by a factor of two thanks to the RF frequency doubling using optical means. On the other hand, compared to [7] and [13], the proposed scheme is less sensitive to fiber chromatic dispersion because the generated RoF signal is not transmitted over a long fiber span up to the fiber cut (mm-wave bridge). In addition, the network is modified only at the two sides of the fiber cut, leaving the rest of the network unaltered, which ensures compatibility with the previously implemented network. However, the feasibility of the proposed scheme is still uncertain, as well as the wireless range achievable and the maximum fiber spans that can be connected. In order to elucidate these points, the proposed scheme has been tested using VPI Transmission Maker, which has been fed with realistic parameters obtained from commercial data sheets. Numerical results reveal the potential of this approach not only as an emergency link but also as early deployment or low-cost infrastructure for both G-PON and XG-PON. A BER below 10^{-9} has been obtained for G-PON NRZ-OOK transmission using the 81-86 GHz mm-wave band with a minimum required wireless link gain (WLG) of –55 dB and XG-PON in the 102-109.5 GHz band with a WLG of –35 dB. Simulation results also show that fiber cuts closer to the ONU degrade more significantly the system performance, causing a penalty in the required WLG.

The paper is organized as follows: Section 2 describes in more detail the proposed mm-wave bridge, the PON signals to be transmitted, and the potential mm-wave bands. The simulation setup is introduced in Section 3, paying special attention to the electrical components. In Section 4, numerical results are presented and discussed, and Section 5 concludes the paper.

2. Photonic mm-wave bridge and PON signals

This section is divided into three subsections: first, the novel photonic mm-wave bridge is described. A second subsection briefly explains the PON signals that are considered in this work, whereas a third subsection is dedicated to the discussion on the potential mm-wave bands for each PON standard.

2.1. Photonic mm-wave bridge architecture

A network implementation based on the proposed photonic mm-wave bridge is sketched in Fig. 1. The downlink PON signal is generated at the optical line terminal (OLT) and transmitted to the optical network units (ONU) using a passive distribution network that includes a first fiber span, a 1×64 splitter, and a second fiber span. In PON networks, the fiber span connecting the OLT and the splitter is specially critical because, if it is sectioned, all the ONUs served by the OLT run out of service.

Therefore, if the physical continuity of the first fiber is compromised because of an incident or if geographical constraints hamper its implementation, the mm-wave bridge can be used to create an alternative high-capacity wireless link. In the mm-wave bridge transmitter, the power of the incoming PON signal is first optically amplified using a semiconductor optical amplifier (SOA). The signal is subsequently remodulated by a MZM, which is biased at zero-intensity point in order to perform RF frequency doubling by optical means, thus relaxing the required modulation bandwidth by a factor of 2 [16]. In this way, after the MZM, two sidebands separated by the desired RF frequency are obtained. These sidebands are photodetected using a broad-bandwidth PD. Once in the electrical domain, the signal is amplified by a HPA and radiated employing a highly directive antenna.

At the mm-wave receiver, the signal is amplified by a low-noise amplifier (LNA) before being downconverted using, for instance, an envelope detector (ED). Afterwards, a gain-controlled amplifier (GCA) conditions the signal strength to get the optimum power level for the electro-optical converter. The

Table 1: Allowed bands for G-PON and XG-PON.

PON	Bitrate	BW (GHz)		57-64 GHz		71-76 GHz		81-86 GHz		92-94 GHz		94.1-100 GHz		102-109.5 GHz	
standard	(Gbps)	DSB	SSB	DSB	SSB	DSB	SSB	DSB	SSB	DSB	SSB	DSB	SSB	DSB	SSB
G-PON (G.984)	2.5	3.75	1.88	✓	✓	✓	✓	✓	✓	✗	✓	✓	✓	✓	✓
XG-PON (G.987)	10	15	7.5	✗	✗	✗	✗	✗	✗	✗	✗	✗	✗	✗	✓

electro-optical conversion can be accomplished either by directly or externally modulating a diode laser. After converted back to the optical domain, the signal is transmitted to the ONU.

2.2. PON signals

In this work, two different PON signals are considered: (i) G-PON, corresponding to the ITU-T G984 standard [4], operating at bit rates of 2.488 and 1.244 Gbps for the downlink and uplink, respectively, and (ii) XG-PON, ITU-T G.987 [5], with 10-Gbps downlink and 2.5-Gbps uplink. Even if recently deployed PON networks are mainly XG-PON, we also study the case of G-PON since a part of the installed PON infrastructure still follows this standard. In both cases, the optical signal is amplitude-modulated employing non-return-to-zero (NRZ) on-off keying (OOK).

NRZ-OOK is, from the point of view of the occupied bandwidth, the most challenging format. For the same bit rate, modulation formats with higher spectral efficiency may offer more flexibility in the selection of the mm-wave band and, consequently, an extra degree of freedom to choose the optimum electronics. It is envisaged, then, that the presented mm-wave bridge will be also capable of operating with emerging PON proposals with spectrally-efficient modulation formats, *e.g.* direct detection orthogonal frequency division multiplexing (DD-OFDM) [17]. In regards to PON systems with wavelength division multiplexing (WDM) [2], the proposed bridge could be upgraded to create multiple links by taking advantage of space multiplication in the wireless domain. The performance of the bridge in PON networks using a more advanced modulation formats and WDM are left as future work.

2.3. mm-wave band selection

There are several unlicensed bands in the mm-wave region that are candidate to accommodate such high-capacity RF signal [14]: the well-known 60-GHz band ranging from 57 to 64 GHz (in Europe and USA), two 5-GHz bands around 73.5 and 83.5 GHz, a relatively narrow 2-GHz band at 91 GHz, a 5.9-GHz band between 94.1 and 100 GHz, and a continuous 7.5-GHz band centered at 107.25 GHz. These unlicensed bands impose bandwidth constraints on the generated RF signals that, alongside with the frequency dependency of the electronics performance and the WLG, constitute important factors in choosing the optimum transmission band.

The bandwidth of the radiated RF signal depends on the optical bandwidth, and whether the photogenerated signal is filtered to generate a single sideband (SSB) or double sideband (DSB). In particular for, NRZ-OOK optical signals that results in electrical ASK signals, the DSB and SSB 3-dB bandwidths of the radiated signal are given by:

$$BW_{DSB} = 1.5 \cdot R \quad (1)$$

and

$$BW_{SSB} = 0.75 \cdot R, \quad (2)$$

where R represents the bitrate of the transmitted signal. Therefore, the DSB bandwidth of G-PON is 3.75 GHz and the SSB bandwidth is 1.875 GHz, whereas for XG-PON, the DSB and SSB bandwidths are 15 and 7.5 GHz, respectively. Since the bandwidth occupied by G-PON is half the occupied by XG-PON, the latter is more difficult to be accommodated in the unlicensed bands.

Table 1 presents the allowable bands for the wireless transmission of both G-PON and XG-PON, considering DSB and SSB transmission. It is clear that, a G-PON signal can be converted to the electrical domain and transmitted in any of the unlicensed bands. It is even unnecessary to resort to SSB, except in the 90-92 GHz band. In XG-PON systems, there is not any band capable of accommodating DSB transmission and only one band satisfies the bandwidth

requirement, the 102-109.5 GHz band, while the 57-64 GHz almost meets this criterion. In both G-PON and XG-PON systems is not clear a priori what is the optimum band, but it requires simulations.

2.4. Performance metrics

In order to assess the performance of the system based on the proposed mm-wave bridge we will employ the bit error rate (BER). This is an intuitive metric that is usually estimated by two methods: it can be calculated by error counting comparing the transmitted and the received bit sequences. For low BER values, however, this method requires a large number of bits to be simulated. An alternative estimation approach for binary signals is the so-called Q-factor method, where BER is estimated by calculating the average and standard deviation values of the *high* and *low* levels. The Q-factor method is useful in systems limited by additive noise as in our case where the main source of noise is the noise induced by the electrical components of the bridge. The Q-factor is directly related not only to the BER but also to the signal-to-noise ratio (SNR) which is another common metric in noise limited systems. The Q-factor is related to the SNR through [18]:

$$Q = \frac{1}{\sqrt{SNR}}, \tag{3}$$

and, therefore, BER can be expressed both in terms of the Q-factor or SNR as:

$$BER = \frac{1}{2}\mathrm{erfc}\left(\frac{Q}{\sqrt{2}}\right) = \frac{1}{2}\mathrm{erfc}\left(\frac{1}{\sqrt{2 \cdot SNR}}\right), \tag{4}$$

where erfc is the complimentary error function.

Even if BER is a useful metric for the overall system, it may not be the best choice to characterize the noisy bridge. For that purpose, in Subsection 4.4, we use another metric, i.e. noise figure (NF), which accounts for the SNR degradation when the signal passes through a noise device. Thus, NF can be calculated as:

$$NF(dB) = 10\log_{10}\left(\frac{SNR_{in}}{SNR_{out}}\right), \tag{5}$$

where SNR_{in} and SNR_{out} are the SNR (in linear scale) at the input and output, respectively.

3. Simulation setup

The technical feasibility of the proposed architecture was tested using VPI TransmissionMaker 9.2. Figure 2 shows the simulation setup alongside with some sampling spectra at different points of the system.

In the OLT, a 2^{14}-bit pseudorandom binary sequence (PRBS) was generated in each run and coded into an electrical signal using NRZ format with a bit rate of 2.5 (10) Gbps for PON (XG-PON). A second-order low-pass filter with a bandwidth of 0.75 times the bit rate of the signal was used consider the bandwidth limitation of the OLT electrical equipment and to limit the occupied bandwidth.

The signal was then converted to the optical domain using direct modulation (G-PON), or external modulation (XG-PON). The directly modulated laser was modeled using the rate equations that relate the complex field and

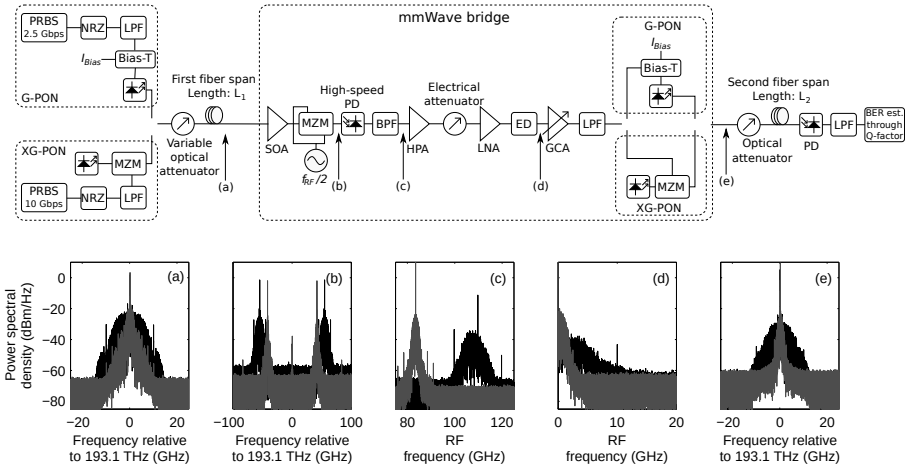

Figure 2: Simulation setup indicating the modules for G-PON and XG-PON. PRBS: Pseudo-random bit sequence generator, NRZ: electrical nonreturn-to-zero modulator, LPF: low-pass filter, MZM: Mach-Zehnder modulator, PD: Photodiode, BPF:bandpass filter, HPA: high-power amplifier, LNA: low-noise amplifier, ED: envelope-detector, GCA: gain-controlled amplifier. Spectra at different points of the system (grey is for G-PON, whereas black is for XG-PON): (a) incoming G/XG-PON signal, (b) remodulated signal, (c) generated mm-wave signal, (d) downconverted signal, and (e) transmitted G/XG-PON signal.

Table 2: Simulation parameters

	Parameter	**Value**	**Unit**
General param.	Bit rate	2.5/10	Gbps
	Number of bits	2^{14}	–
	Samples per symbol	32	–
	Time window	13.1/3.28	μs
Laser	Nominal wavelength	1550	nm
	RIN	-150	dB/Hz
	Linewidth	1	MHz
	Threshold current	20	mA
	Adiabatic chirp	10	GHz/W
	Slope efficiency	0.3	W/A
SSMF	Attenuation	0.2	dB/km
	Dispersion coef.	16	ps/nm/km
	Dispersion slope	80	ps/nm^2/km
	Kerr coeficient	0.026	nm^2/W
	Core area	80	μm^2
MZM	Insertion loss	4	dB
	Bias voltage	2.5	V
	Extinction ratio	40	dB

carrier density within the single-mode laser cavity. With the parameters listed in Table 2, the laser exhibits a threshold current of 20 mA and a current slope of 0.3 mW/mA, which are reasonable values for commercial distributed feedback (DFB) lasers. The driving electrical signal was amplified and combined with a bias current resulting in a signal varying from 3 to 5 times the laser threshold current. On the other hand, for XG-PON, a MZM with an extinction ratio of 40 dB and an insertion loss of 4 dB was used to externally modulate the output of a laser with constant driving current (5 times the threshold current). In order to maximize the modulation depth of the optical signal, the MZM was set at the quadrature point. The resulting optical average power levels were 12.58 dBm

and 7.85 dBm for direct and external modulation, respectively.

The standard single mode fiber (SSMF) connecting the OLT with the bridge, and the bridge with the ONU, was simulated using the split step Fourier transform (Table 2), which has shown to realistically mimic the behavior of dispersive nonlinear systems [19]. The 1×64 splitter was modeled inserting a 20-dB optical attenuator that accounts for the splitting loss as well as for other impairments such as insertion and connection losses. In addition, a variable optical attenuator (VOA) was included at the output of the OLT to control the launched optical power at the input of the first fiber span.

Regarding the mm-wave bridge components, the broad-bandwidth MZM of the bridge had a 6-dB insertion loss and a 40-dB extinction ratio. The SOA was configured in power clamped mode with an output power of 15 dBm, a maximum gain of 20 dB, and a noise figure of 9 dB. This ensures that the SOA does not enter into saturation and, consequently, no pulse distortion is expected. In addition, the short optical path from the SOA up to the photodetection within the bridge transmitter avoids that the SOA-induced chirp to be converted into amplitude modulation and the subsequent distortion in the pulse shape. The optical to electrical conversion was made employing a high-speed PD with a responsivity that depends on its electrical bandwidth (Table 3), a 20 $pA/\sqrt{Hz}$ thermal noise current spectral density, and shot noise. The parameters of most of the electrical components highly depend on the mm-wave band, as can be seen in Table 3. The electro-optical conversion in the mm-wave bridge was accomplished in the same way as in the OLT, that is, using direct modulation for 2.5 Gbps and external modulation for 10 Gbps. In order to optimize the modulation index, the driving power input at the directly modulated laser or external modulator was controlled using a gain controlled amplifier (GCA), after which a low-pass filter with a bandwidth of 0.75 times the signal bitrate removed the out of band noise.

Finally, the signal was detected at the ONU, which is based on a conventional direct detection scheme. The PD in the ONU had a 10-GHz bandwidth, a responsivity of 0.9 mA/mW, and a thermal noise current density of 10 $pA/\sqrt{Hz}$.

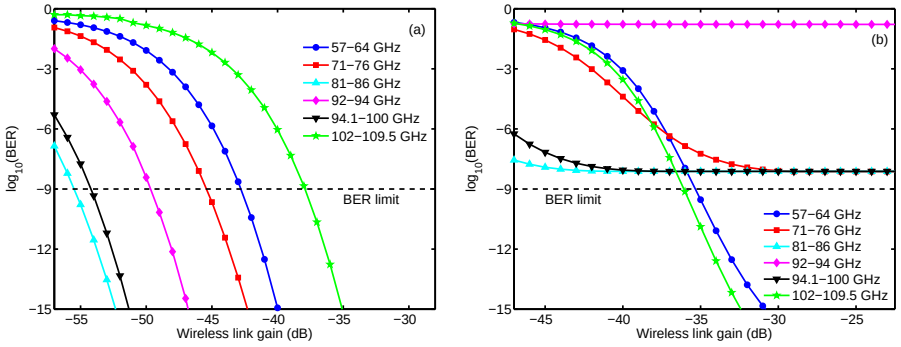

Figure 3: BER in terms of the wireless link gain for the different mm-wave bands: (a) G-PON and (b) XG-PON.

Since the target bit error rate is very low, 10^{-9}, error counting was unfeasible and BER was estimated through the mentioned Q-factor method [18].

3.1. Electrical components

The high-frequency components, both amplifiers and EDs, are modeled using the parameters obtained from data sheets supplied by Millitech [20], which is a manufacturer that has a portfolio covering the different bands for both amplifiers and EDs. The broad-bandwidth PD specifications are obtained from different vendors depending on availability and performance. For less than 90 GHz, we use the data sheet from Henrich Hertz Institute (HHI) [21], while for higher frequencies we select products from Finisar [22]. Table 3 lists the most important parameters for each component and frequency band. For the HPA, both the gain and the 1-dB compression point[5] are given; whereas for the LNA, the gain and the noise figure are given. The reason for this difference is that the main impairment in the HPA is the nonlinear distortion while for the LNA the main nuisance is noise. Regarding the envelope detector, the key figure of merit is the sensitivity, which is typically expressed in mV/W.

[5]The output power at which the power level is reduced 1 dB from the linear response, often considered the maximum output power without significant distortion

Table 3: Parameters of the electrical components.

Device	Parameter	57-64 GHz	71-76 GHz	81-86 GHz	92-94 GHz	94.1-100 GHz	102-109.5 GHz
HPA	Model	AMP-15-03100	AMP-12-02280	AMP-12-40100	AMP-10-41030	AMP-10-02580	AMP-08-40110
	Gain (dB)	21	22	29	27	16	20
	1dBCP (dBm)	17.5	15	27.5	30	15	18.5
	Consumption (W)	1.875	1.875	–	24.5	1.125	–
LNA	Model	LNA-15-03090	LNA-12-02190	LNA-12-02220	LNA-10-03130	LNA-10-02130	LNA-08-03210
	Gain (dB)	19	12	15.5	19	30	17
	NF (dB)	4.8	5.5	3.8	4.6	5.5	8.0
	Consumption (W)	0.45	0.375	0.9	0.375	0.75	0.3
ED	Model	DET-15	DET-12	DET-10	DET-08	DET-08	DET-08
	Sensitivity (mV/W)	850	850	1000	1000	1000	1000
	Max. input (dBm)	-10	-10	-10	-10	-10	-10
PD	Model	HHI	HHI	HHI	XPDV4120R	XPDV4120R	XPDV412xR
	Responsivity (A/W)	0.6	0.6	0.6	0.6	0.6	0.5
	Max. output (dBm)	12	12	12	7.5	7.5	7.5

3.2. Wireless channel model

Given the high operation frequency in the RF stage (81-86 GHz for G-PON and 102-109.5 GHz for XG-PON), we will assume a point-to-point directive line-of-sight (LoS) link with unblocked first Fresnel zone [23]. In clear terrestrial fixed links, reflections from any objects, including ground, present extremely low power and, consequently, there will not be multi-path effect. Additionally, since there is not moving scatterers within the line-of-sight and the relative position of the transmitter and receiver is fixed, no Doppler shift of spread are present. In this scenario, the LoS wireless link can be modeled as a flat attenuation, which is usually characterized by the wireless link gain (WLG). Generally, the WLG accounts not only for the path-loss but also for the transmitter and receiver effective antenna gains, G_{Tx} and G_{Rx} (it is worth noting that the term *effective* includes any penalty in the gain due to misalignment). We will present many of the results in terms of the WLG, which according to the Friss formula can

be calculated as:

$$WLG|_{dB} = G_{Tx}|_{dB} + G_{Rx}|_{dB} - Loss_{Path}|_{dB}. \quad (6)$$

It is important to note that we have neglected atmospheric losses since for the frequencies and distances we are considering free-space loss dominates [23]. To accomplish the WLG to distance conversion, we employed 40-dBi antennas taken from the data sheet of Quinstar [24].

4. Results and discussion

In this section we first discuss the mm-wave band selection for G-PON and XG-PON. Afterwards, the photonic bridge is optimized for different received optical power levels and the effects of the fiber spans is analyzed for both standards. Finally, regression curves for the equivalent noise figure (NF) of the bridge are presented.

4.1. Band selection

According to Table 1, there are multiple choices to accommodate G-PON signals in the unlicensed mm-wave bands. The optimal selection was based on the performance of the electronic devices at different bands. Figure 3(a) shows the BER in terms of the WLG for the different unlicensed bands in an optical back-to-back configuration. The importance of band selection appears clear in this figure, showing a WLG difference between the best and worst bands of 17 dB at the BER threshold. Results reveal that the minimum required WLG is achieved in the 81-86 GHz band, which is explained by the high performance of electronics in this band: high 1-dB compression point of the HPA, and low NF of the LNA.

Regarding XG-PON, band-limitation plays an important role. Recall that the 10-Gbps signal occupies a bandwidth of 7.5 GHz. So, as can be seen in Fig. 3(b), only the transmission at the 57-64 GHz and 102-109.5 GHz bands achieves the required BER. This was an expected outcome since these bands

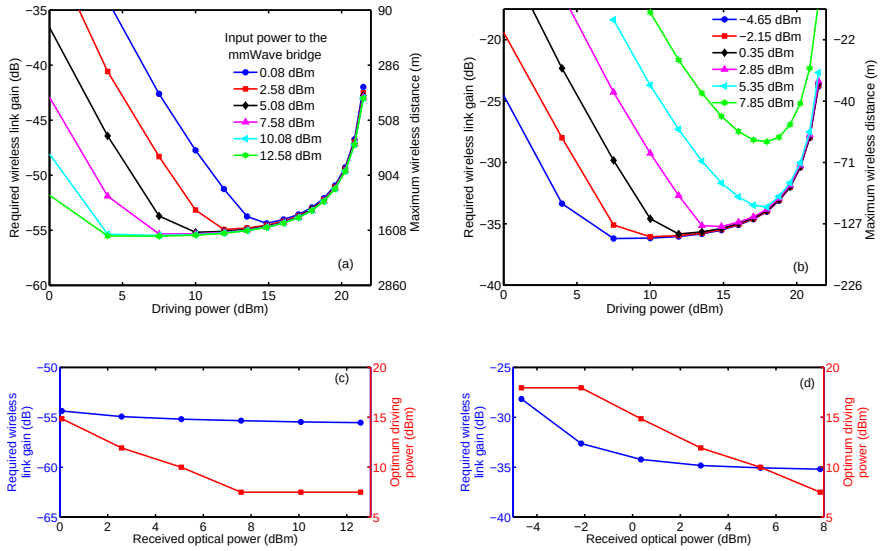

Figure 4: Optimization of the driving power of the microwave tone at the MZM. Required wireless link gain to achieve a BER of 10^{-9} for different optical power at the input of the mm-wave bridge in terms of the driving power for (a) G-PON and (b) XG-PON. Required wireless link gain and optimum driving power for (c) G-PON and (d) XG-PON.

are the widest. In the rest of the bands, an important percentage of the signal power is filtered out.

In conclusion, the optimum band for the transmission of the G-PON signal is the 81-86 GHz band, whereas for XG-PON, the optimum mm-wave band is 102-109.5 GHz.

4.2. Bridge optimization

The noise added by the bridge components, such as the PD and amplifiers, is the main physical impairment that degrades the system performance. Its impact can be reduced by increasing the driving power of the MZM. However, given the nonlinear response of the MZM, a high driving power will induce nonlinear distortion. Therefore, the performance of the proposed architecture is ultimately limited by the combined effects of noise and nonlinear distortion.

Figures 4(a-d) presents the required WLG and its corresponding maximum

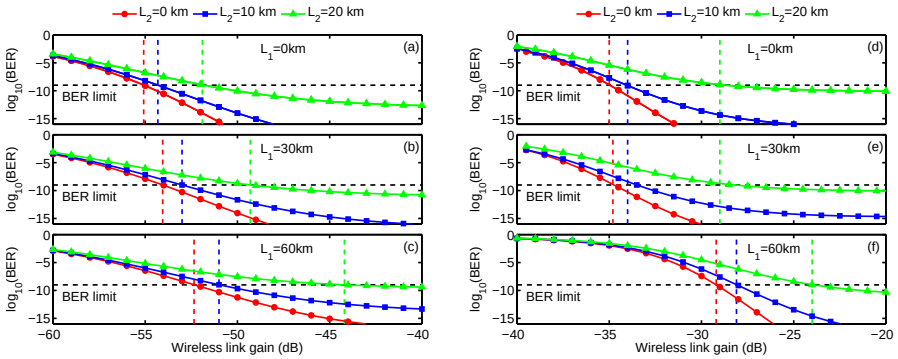

Figure 5: BER in terms of the wireless link gain for different combinations of fiber span lengths L_1 and L_2 (a), (b), (c) are for G-PON with $L_1 = 0$ km, $L_1 = 30$ km, and $L_1 = 30$ km, respectively, whereas (d), (e), and (f) are for XG-PON with the same L_1 values.

range as a function of the electrical driving power and the optical received power at the bridge. We used the VOA between the OLT and the bridge to sweep the received power, considering attenuations between 0 and 12.5 dB that approximately correspond to the loss of fibers of 0 to 60 km. For both G-PON and XG-PON, Figs. 4(a-b) shows that for low driving powers, the required WLG decreases at higher optical input powers, while for high driving powers, the required WLG is independent of the optical input power in G-PON; but for XG-PON, a 60 km fiber length increases the required WLG. Notice that the maximum wireless distance is an order of magnitude less for XG-PON.

In Figs. 4(c-d) the optimal driving power and required WLG are shown in terms of the received optical power. Comparing Fig. 4(c) and Fig. 4(d), we conclude that WLG suffers only a 1.5 dB penalty when decreasing the power from 8 to –4 dBm for G-PON. For XG-PON this penalty increases to 7 dB. These curves are employed in the next subsection to choose the driving power depending on the fiber length under study.

4.3. Influence of the fiber cut position on the WLG

The minimum WLG presented in Fig. 4(c) and Fig. 4(d) are for optical back-to-back, that is, without including optical fiber. In order to analyze the effect

of both fiber spans, Figs. 5(a-f) show the BER curves for different combinations of fiber lengths. For G-PON, the sequence of Figs. 5(a-c) shows a progressive degradation of the system performance as the length of the first fiber span is increased. However, this is not the case in XG-PON where Figs. 5(d-e) show a minimal performance degradation if the length of the first fiber link is shorter than 30 km. It is important to note that in both G-PON and XG-PON, the performance degrades much faster as the second fiber span length increases. This can be explained by the fact that in the second span, a 20-dB attenuator is included and, therefore, the system is more sensitive to losses in this span. The effect of the combination of different fiber span lengths can be appreciated more clearly in Fig. 6(a) and Fig. 6(b), where contour plots of the required WLG for G-PON and XG-PON are presented. As expected from Figs. 5(a-f), in G-PON, a longer first fiber span allows a shorter second fiber span to meet the BER requirement. In contrast, in XG-PON, the performance remains independent of the first fiber span up to 30 km, after which, performance degrades significantly faster than in the case of G-PON. This behavior can be explained by noting that for short first spans, the generated RF power is limited by the output power of the SOA. Thus, it is independent of the attenuation in the first span and, consequently, of its length. For longer first span lengths, the RF power is limited by the gain of the SOA and the power and its input, leading to a dependence

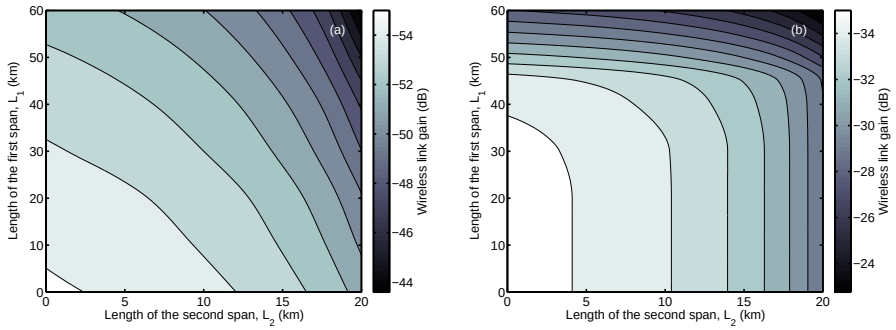

Figure 6: Contour graphs for the minimum required wireless link gain to achieve a BER of 10^{-9} with different fiber lengths of L_1 and L_2 for (a) G-PON and (b) XG-PON.

on the first fiber span length.

4.4. Modeling the bridge as a noisy power-clamped amplifier

In this subsection, we propose a simplified model of the bridge, which has a twofold goal: first, to deep our knowledge of the signal degradation induced by the bridge and, second, to develop a model that can be used in a SNR budget analysis. Since the SNR depends on the signal and noise power, we need to model the output power and the amount of noise added by the bridge.

As explained in Section 2 the output power is fixed at the electrical-to-optical conversion stage. Hence, the bridge can be seen as a gain-controlled amplifier, or, equivalently, as an amplifier whose output power is clamped. The output powers are 12.58 and 7.85 dBm for G-PON and XG-PON, respectively.

In regards to the added noise, we characterize it in terms of the noise figure (NF), which is defined as the difference in dB between the electrical SNR before and after the device under test [18][6]. It is expected that the NF will be highly dependent on the WLG since, at low values, the LNA will add significant noise, degrading the SNR at the output of the bridge. This assumption is supported by the curves presented in Fig. 7 for G-PON and XG-PON.

In both cases three different regions can be identified:

- For low WLG values, the NF is highly dependent on the WLG, which can be explained by noting that at low WLGs, the main noise source is the LNA.

- At high WLGs, the NF does not depend on the WLG. This can be attributed to the fact that, as the WLG increases, the received power at the mm-wave receiver also rises. Therefore, the LNA is not the main noise source any more and the thermal and shot noise of the PD dominate.

- For moderate WLGs, the SNR degradation due to the LNA and the PD are comparable. For these WLG values, the NF is not linear but may be

[6]The conversion to the electric domain was performed using the same PD as in the ONU.

approximated by a quadratic curve.

Although in both G-PON and XG-PON the three mentioned regions can be identified, the regression parameters in each region, as well as the boundaries between regions differ. For G-PON, the region where the main noise source is the LNA covers WLG up to −56.1 dB; while in XG-PON, this region is up to −42.3 dB. In addition, the slope is sharper in the case of XG-PON, which indicates that XG-PON is more sensitive to the LNA noise. For WLGs ranging from −56.1 dB to −35.7 dB the transmission of G-PON is severely affected by both the PD and the LNA noise. In XG-PON, this region spreads between −42.3 and −26.7 dB. At WLGs above −35.7 dB (−26.7 dB) the G-PON (XG-PON) NF is mainly affected by the PD noise.

The data presented in Fig. 7 can be used as a look-up table or, alternatively, a piecewise regression can be performed to facilitate its use. Eq. 4 and Eq. 5 present the regressions for G-PON and XG-PON, respectively.

$$NF_G = \begin{cases} -0.933 \cdot WLG - 24.88 & WLG \leq -56.1 \\ \sqrt{30.11^2 - (WLG + 35.57)^2} + 49.47 & -56.1 \leq WLG \leq -35.7 \\ 19.37 & -35.7 \leq WLG \end{cases} \quad (7)$$

$$NF_{XG} = \begin{cases} -1.7388 \cdot WLG - 44.49 & WLG \leq -42.3 \\ \sqrt{17.95^2 - (WLG + 26.65)^2} + 37.95 & -42.3 \leq WLG \leq -26.7 \\ 19.95 & -26.7 \leq WLG \end{cases} \quad (8)$$

5. Conclusions

A mm-wave bridge based RF frequency doubling is proposed to overcome accidental fiber cuts in optical access networks. Simulation carried out in VPI Transmission Maker revealed that the photonic mm-wave bridge is capable of converting conventional PON signals at 2.5 and 10 Gbps bitrates and transmit them wirelessly at 81-86 GHz and 102-109.5 GHz keeping a BER lower than

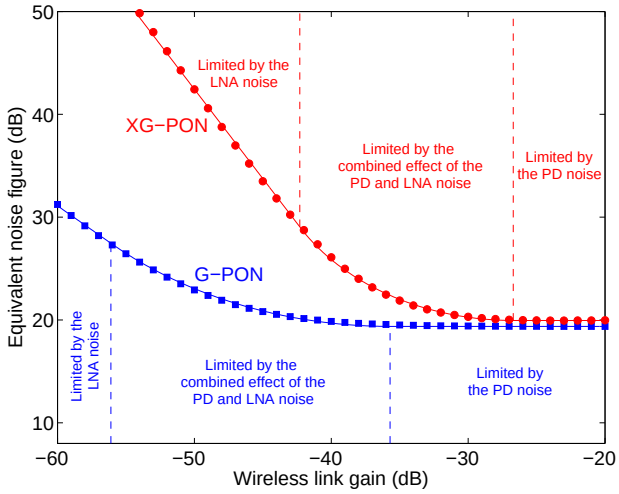

Figure 7: Equivalent noise figure in terms of the wireless link gain for G-PON and XG-PON.

10^{-9} provided that the WLG is higher than –55 and –35 dB, respectively. Results also show that when using the proposed scheme, the closer the fiber cut to the ONU is, the more the system performance is deteriorated.

6. Acknowledgements

This work has been partially funded by FAPESP under grant 2015/04113-0, CONACyT and EU Horizon 2020 research and innovation programme under the Marie Skodowska-Curie grant agreement No 713567, SFI CONNECT Research Centre and Sterlite Techn. Ltd.

7. References

[1] J. M. Simmons, Optical Network Design and Planning, 2nd ed. Springer (2014).

[2] T. Koonen, Trends in optical access and in-building networks, Proceedings of European Conference on Optical Communications (2008) 1-31. doi: 10.1109/ECOC.2008.4729555.

[3] E. Trojer, S. Dahlfort, D. Hood, and H. Mickelsson, Current and next-generation PONs: A technical overview of present and future PON technology, Ericsson, Tech. Rep. (2008) 64-69.

[4] ITU-T Rec. G.984 series: Gigabit-capable passive optical networks (G-PON), International Telecommunication Union 45(3), Tech. Rep. (2008) S17-S25. doi: 10.1109/MCOM.2007.344582.

[5] ITU-T Rec. G.987 series: 10-Gibabit-capable passive optical networks (XG-PON), International Telecommunication Union, Tech. Rep. 79(3) (2012) 117-122.

[6] Y. Sambo, M. Shakir, K. Qaraqe, E. Serpedin, and M. Imran, Expanding cellular coverage via cell-edge deployment in heterogeneous networks: spectral efficiency and backhaul power consumption perspectives, IEEE Communications Magazine 52(6) (2014) 140-149. doi: 10.1109/MCOM.2014.6829956.

[7] K. Kitayama, *et al.*, High-speed optical and millimeter-wave wireless link for disaster recovery, Globecom Workshops (GC Wkshps), (2015).

[8] T. Kawanishi, Transparent waveform transfer for resilient low-latency links, IEEE Photonics Society Newsletter 28(4) (2014) 4-8.

[9] D. Zhou and S. Subramaniam, Survivability in optical networks, Network, IEEE 14(6) (2000) 16-23. doi: 10.1109/65.885666.

[10] J. Chen and L. Wosinska, Analysis of protection schemes in PON compatible with smooth migration from TDM-PON to hybrid WDM/TDM-PON, Journal of Optical Networking 6(5) (2007) 514-526. doi: 10.1364/JON.6.000514.

[11] C. Mas-Machuca, J. Chen, and L. Wosinska, PON protection architectures achieving total cost reduction, Proceedings of Asia Communications and Photonics (2010) 707-708. doi: 10.1109/ACP.2010.5682700.

[12] S. Koenig, J. Antes, D. Lopez-Diaz, I. Kallfass, T. Zwick, C. Koos, W. Freude, and J. Leuthold, High-speed wireless bridge at 220 GHz connecting two fiber-optic links each spanning up to 20 km, Proceedings of Optical Fiber Communication (OFC) (2012) 1-3.

[13] A. Lebedev, X. Pang, J. Vegas Olmos, M. Beltran, R. Llorente, S. Forchhammer, and I. Tafur Monroy, Feasibility study and experimental verification of simplified fiber-supported 60-GHz picocell mobile backhaul links, Photonics Journal, IEEE 5(4) (2013) 7 200 913-7 200 913. doi: 10.1109/JPHOT.2013.2277011.

[14] Z. Pi and F. Khan, An introduction to millimeter-wave mobile broadband systems, IEEE Communications Magazine 49(6) (2011) 101-107. doi: 10.1109/MCOM.2011.5783993.

[15] J. Beas, G. Castañón, I. Aldaya, G. Campuzano, and Aragón-Zavala, Millimeter-wave frequency radio over fiber: a survey, IEEE Communication Surveys and Tutorials, PP(99) (2013) 1-27. doi: 10.1109/SURV.2013.013013.00135.

[16] Z. Jia, J. Yu, G. Ellinas, and G. K. Chang, Key enabling technologies for optical-wireless networks: Optical millimeter-wave generation, wavelength reuse, and architecture, Journal of Lightwave Technology 25(11) (2007) 3452-3471. doi: 10.1109/JLT.2007.909201.

[17] J. M. Tang, R. P. Giddings, X. Q. Jin, J. L. Wei, X. Zheng, E. Giacoumidis, E. Hugues-Salas, Y. Hong, C. Shu, J. Groenewald, and K. Muthusamy, Real-time optical OFDM transceivers for PON applications, Proceedings of Optical Fiber Communication Conference and (OFC) (2011) 1-3.

[18] G. P. Agrawal, Fiber-Optic Communication Systems. John Wiley and Sons, Inc., 2002.

[19] G. Agrawal, Nonlinear Fiber Optics, 3rd ed. San Diego, CA: Academic Press, 2001.

[20] [Online]. Available: http://www.millitech.com

[21] [Online]. Available: http://www.hhi.fraunhofer.de

[22] [Online]. Available: https://www.finisar.com

[23] S. Saunders and Aragón-Zavala, Antennas and Propagation for Wireless Communication Systems, 2nd ed. Wiley & Sons, 2007.

[24] [Online]. Available: http://quinstar.com